Electrical Power and Energy Systems 152 (2023) 109264

Contents lists available at ScienceDirect

International Journal of Electrical Power and Energy Systems

journal homepage: www.elsevier.com/locate/ijepes

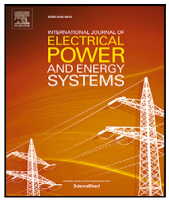

# Voltage and active power local PI control of distributed energy resources based on the effective transfer function method

Giuseppe Fusco, Mario Russo *, Giovanni Mercurio Casolino

*Department of Electrical and Information Engineering, University of Cassino and Southern Lazio, Via G. Di Biasio 43, Cassino (FR), 03043, Italy*

ARTICLE INFO

*Keywords:*
Distributed generation
Voltage and active power regulation
MIMO modeling
Independent SISO design
Control loops interaction
Parameter uncertainties
Robust stability

ABSTRACT

This paper presents the design of local PI regulators to control voltage and active power of the Distributed Energy Resources (DERs) in grid-connected Active Distribution Networks (ADNs). The design is developed based on the proposed Multiple-Input Multiple-Output (MIMO) model of ADN. Firstly, the Relative Gain Array (RGA) matrix is used to address the problem of input–output pairing and to show that the voltage control loops are coupled whereas the active power control loops are decoupled. Subsequently the method of the Effective Open-Loop Transfer Function (EOTF) is used to decompose the multi-loop voltage control system into a set of equivalent Single-Input Single-Output (SISO) loops. Then, each PI regulator is independently designed to fulfill some control objectives dictated by the designer. The proposed design procedure is simple and straightforward. The fixed-parameters PI regulators facilitate the integration of DERs into traditional distribution networks which are usually operated without or with limited communication infrastructure. The simulation results presented for various scenarios of two different ADN confirm that performance objectives and regulation at the desired set-points are achieved in a robust sense.

## 1. Introduction

The long-lasting climate emergency and the present energy crisis, both related to the intensive use of fossil fuels, are strongly driving the transition of distribution systems from traditional passive networks to active grids with high penetration of Distributed Energy Resources (DERs) that exploit Renewable Energy Sources (RESs). New issues in management and control of Active Distribution Networks (ADNs) arise, which are mainly related to system protection [1] (in particular overloads of the lines and components, increase/decrease of short-circuit currents, inverter ride-through capability) and to voltage quality [2] (in particular voltage profiles along the feeders and voltage harmonic distortion). Concerning the latter issue, grid codes and regulatory framework all over the world are introducing requirements for new functionalities of the inverter, which interfaces DERs to the distribution network, so as to provide voltage support [3,4]. In fact, the well-known characteristics of distribution lines, with high R/X ratio, impose to act on both active and reactive powers injected by DERs to support network voltage profiles [5]. Then, the present-day challenge is to effectively include DERs in the voltage control system of the ADN, while guaranteeing the optimal exploitation of RESs.

An overview of the possible control architectures for ADN is presented in [6,7], control strategies for voltage regulation in [8] while paper [9] has investigated pros and cons of a fully decentralized approach. Indeed, from the Distribution System Operator's (DSO) perspective, the choice of the architecture must account for some technical and economical constraints. In particular, distribution systems, especially in LV, are scarcely automated and present a large number of nodes and customers. Then, the best solutions for the DSO must be simple and scalable, should require limited investments in communication infrastructures and tend to a plug-and-play approach for DERs [10]. To achieve the benefits of different architectures while limiting their disadvantages with respect to DSO expectations, the control system is often structured in multiple levels [3,11] or stages [12] or layers [13], each one adopting the best architecture for its specific objective and time horizon. The lower level or layer, that promptly acts as the first stage in the time scale, is typically composed of local closed-loop controllers, each one acting on a single DER. The main advantages of local control structure are the absence of communications infrastructure, thanks to the use of local measurements and actions, and the quick responsiveness. The latter characteristic allows to cope with the rapid fluctuations of RESs, overcoming the limitation of traditional slow-acting voltage regulation devices used in distribution systems, such as on-load tap changers (OLTCs), step voltage regulators and shunt capacitor banks [14].

Focusing on local control of DERs, there are still many challenges that need to be addressed, in particular the adequate setting of the

* Corresponding author.
*E-mail address:* mario.russo@unicas.it (M. Russo).

https://doi.org/10.1016/j.ijepes.2023.109264
Received 20 February 2023; Received in revised form 28 April 2023; Accepted 16 May 2023
Available online 6 June 2023

parameters of local controllers [2], so as to cope with the uncertainty related to RESs [15], to guarantee a stable behavior [5] while reaching a feasible operating point [16]. Concerning the control structure, regulatory standards as well as many DSOs propose Volt/Var droop control [11] for reactive powers and curtailment or delta Volt/Watt control for active powers [10,13]. The problem of adequate selection of the droop parameters, in particular of the slope for the reactive power control, has been studied so as to avoid voltage oscillations [17,18], system instability [19,20] and to cope with DERs interaction [21]. In addition, adaptive approaches have been proposed in [14,22] to account for the changes of the operating conditions of the ADN. The Volt/Var droop control has the advantage of a simple structure and the disadvantage of presenting a steady-state error with respect to the voltage set-point. Moreover, in [21] it has been shown that the larger the number of DERs, the smaller the slop to guarantee stability, and, consequently, the larger the steady-state voltage error. Unfortunately, large steady-state control errors cause the ADN to operate far from the desired feasible conditions; in particular reactive powers may reach DER saturation limits and active powers may be excessively curtailed or varied without respecting predefined rules. Achieving adequate set-points for the voltage and the active power controllers is then a key issue to guarantee the optimal steady-state operating conditions of the ADN. The adequate set-points are typically determined by an upper level or layer, which is implemented by distributed coordination [12,23] requiring communication infrastructure at least among neighboring DERs [16]; in alternative, the set-points are determined by centralized optimization [11,13]. In conclusion, the droop control is becoming inadequate with the increasing penetration of DERs.

To overcome the limitations of the droop control structure, the design of local PI regulators have recently been proposed. The main issue is related to the design of the fixed-parameters of PI regulators which should guarantee performance and system stability under model parameters uncertainty. In details, in [5] the numerical solution of a nonlinear constrained minimization problem gives the gains of a state-feedback controller and parameters of two standard regulators of type PI and I, which realize the dynamic voltage and active-power adjustment. In [24] the PI parameters are updated in an optimization process since the authors claim that fixed-gain PI cannot easily adapt to power changes. A different design approach is employed in [25]; in this paper the PID parameters are tuned using an intelligent adaptive neuro-fuzzy inference system. In [10] the local voltage PI regulator acts on both active and reactive powers according to the following strategy: voltage support with reactive power, single-sided set point tracking of the upper voltage limit, and active power limitation using delta control. Local digital controllers are synchronized so that all input–output updates occur at universal time-discrete instances. Stability is analyzed using a traditional model of the ADN based on the Jacobian matrix of Newton–Raphson load flow, which does not account for the peculiar characteristics of distribution networks. In [11] stability conditions via a discrete-time state-space model are formulated to design the local controllers based on local voltage sensitivities. Then, the discrete-time state-space model is extended for the full system in order to ensure a globally stable control framework.

In summary, although the cited research deals with PI control, there is still a gap between Single-Input Single-Output (SISO) design of PI regulators with fixed-parameters and the design of centralized Multiple-Input Multiple-Output (MIMO) adaptive controllers. Although the former remains the standard for controlling MIMO systems [26] it may not achieve the desired performance and robustness for a strongly-coupled uncertain MIMO process. The latter one is well suited to applications where coupling and uncertainty is present but usually requires a more complex design and is difficult to be implemented in practice, due to the need of high-capacity communication infrastructures. Motivated by these considerations, the aim of this paper is to bridge this gap by proposing a SISO design approach for PI regulators with fixed-parameters which, retaining the simplicity of the procedure, guarantees robustness to parameters uncertainty by accounting for a detailed MIMO model of the process. Moreover, differently from the described papers, the proposed method allows to achieve a desired control performance. In the proposed control scheme, each DER is equipped with two PI regulators which control, respectively, the DER active power and the voltage at the node of connection to the ADN. The design is based on a square MIMO model of the ADN with coupling dynamics causing interactions among control loops. The analysis of these interactions is developed using the Relative Gain Array (RGA) and demonstrates that the active power control loops are decoupled whereas the voltage control loops are strongly coupled. Hence the PI of the active power control loop is independently designed for the corresponding diagonal element of the MIMO model. To retain an independent and easy design also for the PI of the voltage control loop, the Effective Open Transfer Function (EOTF) method [26,27] is employed. Using this method, the MIMO voltage subsystem is converted into several equivalent single loops and then the PI are designed for these single loops. In such a way, the complexity in the design is avoided even in presence of a large number of DERs. The presented SISO procedure guarantees robust performance and stability in spite of interactions among the control loops of each DER and of parameters uncertainty in the MIMO model. Summarizing, the main features of the proposed method, compared with the existing studies, are

- Develop an independent SISO design of local voltage and active-power PI regulators with fixed-parameters using the concept of Effective Transfer Function.
- Present a square MIMO model of the ADN oriented to voltage and active power control of a DER..
- Analyze the internal and external interactions among voltage and active-power control loops which are commonly neglected by most techniques.
- Study the control system robustness and performance in presence of model parameters uncertainty and disturbances.
- Obtain simple control laws whose implementation is oriented to existing ADNs because it does not need additional communication infrastructures.

The rest of this paper is organized as follows. Section 2 illustrates the modeling of the ADN. The design of the local PI controllers is presented in Section 3. Section 4 shows the simulation results. Section 5 summarizes the paper and draws the conclusions.

## 2. Models

The typical configuration of an ADN is radial with feeders; it is supplied by a slack bus at higher voltage level through a substation transformer. The total number of DERs is denoted by $\ell$; the integer $m_j$ represents the number of the network node which the $j$th DER is connected to. Hereafter the model of the DER and of the Distribution Network (DN) without DERs are firstly described and then combined to obtain the overall model of the ADN.

### 2.1. DER

The DER is composed of a RES, that may include also an Energy Storage System (ESS). Small-sized RES conversion systems are typically connected to a DC bus which is interfaced to the network by an inverter, namely a Voltage Source Converter (VSC); in the remainder such a configuration is assumed. The VSC is synchronized to the voltage network by a Phase Lock Loop (PLL). The commands to be sent to the VSC are references expressed as components in the $dq$ frame; they refer to the VSC voltages or currents according to whether the VSC is equipped with voltage or current control loops. In practical applications, the voltage control solution is not adopted because it does not guarantee that the inverter currents are limited and, consequently, overcurrents may be generated [28]. Then, the most widely adopted configuration is

the current-controlled VSC, whichever the type of the RES conversion system connected to the DC bus. Such a configuration allows to achieve fast action by DERs. The resulting responsiveness of DER control is much higher than the one of traditional voltage regulating devices and the related interaction can then be neglected [14,29].

Referring to the $j$th DER, the current-controlled VSC can be modeled by its closed-loop dynamics modeled with SISO or Two-Inputs Two-Outputs (TITO) model [19,30,31]. If the VSC is equipped with an L-type output filter, it is possible to lump the filter's parameters in those of the lines connected to the VSC. In our paper, the current reference values $u_{jd}$, $u_{jq}$ are the inputs and the actual currents $i_{jd}$, $i_{jq}$ injected by the DER into the network the outputs. The electrical quantities are represented by their components in the $d-q$ coordinate frame which is synchronized with the network voltage $v_{m_j}$. According to [5], the following TITO model is adopted

$$\begin{pmatrix} i_{jd} & i_{jq} \end{pmatrix}^{\mathrm{T}} = \mathbf{G}_j(s) \begin{pmatrix} u_{jd} & u_{jq} \end{pmatrix}^{\mathrm{T}} \tag{1}$$

where the transfer functions matrix $\mathbf{G}_j(s)$ is expressed by

$$\mathbf{G}_j(s) = \begin{pmatrix} \dfrac{1}{1+s\,\tau_{jd}} & \dfrac{-k_{j1}\,s}{(1+s\,\tau_{j1})(1+s\,\tau_{j2})} \\ \dfrac{k_{j2}\,s}{(1+s\,\tau_{j3})(1+s\,\tau_{j4})} & \dfrac{1}{1+s\,\tau_{jq}} \end{pmatrix} \quad j = 1, \dots \ell \tag{2}$$

In (2), the diagonal transfer functions model the dynamics along the $d-q$ axes, while the off-diagonal transfer functions the cross-coupling dynamics. These latter dynamics are relevant in the case of a DER connected to a weak distribution network [32].

Assuming to use *per unit* (p.u.) quantities, the active and reactive powers ($p_j$, $q_j$) injected by the VSC are

$$p_j = v_{m_j}\, i_{jd} \qquad q_j = v_{m_j}\, i_{jq} \tag{3}$$

The linearization of (3) around an initial operating point yields the variational model

$$\begin{aligned} \Delta p_j &= v^0_{m_j}\, \Delta i_{jd} + i^0_{jd}\, \Delta v_{m_j} \\ \Delta q_j &= v^0_{m_j}\, \Delta i_{jq} + i^0_{jq}\, \Delta v_{m_j} \end{aligned} \tag{4}$$

where the operating point is denoted by subscript "0" and deviations around the operating point are demonstrated by the prefix "$\Delta$".

Considering all the $\ell$ DERs connected to the network, models (1) can be written in compact form as

$$\boldsymbol{i} = \mathbf{G}(s)\, \boldsymbol{u} \tag{5}$$

with

$$\begin{aligned} \boldsymbol{i} &= \begin{pmatrix} i_{1d} & i_{1q} & \dots & i_{\ell d} & i_{\ell q} \end{pmatrix}^{\mathrm{T}} \\ \boldsymbol{u} &= \begin{pmatrix} u_{1d} & u_{1q} & \dots & u_{\ell d} & u_{\ell q} \end{pmatrix}^{\mathrm{T}} \\ \mathbf{G}(s) &= \mathrm{diag}\{\mathbf{G}_j(s)\} \end{aligned} \tag{6}$$

and models (4) as

$$\begin{aligned} \Delta \boldsymbol{p} &= \boldsymbol{V}^0\, \Delta \boldsymbol{i}_d + \mathbf{I}^0_d\, \Delta \boldsymbol{v} \\ \Delta \boldsymbol{q} &= \boldsymbol{V}^0\, \Delta \boldsymbol{i}_q + \mathbf{I}^0_q\, \Delta \boldsymbol{v} \end{aligned} \tag{7}$$

where

$$\begin{aligned} &\boldsymbol{i}_d = (i_{1d} \dots i_{\ell d})^{\mathrm{T}} \quad \boldsymbol{i}_q = (i_{1q} \dots i_{\ell q})^{\mathrm{T}} \quad \boldsymbol{v} = (v_{m_1} \dots v_{m_\ell})^{\mathrm{T}} \\ &\boldsymbol{p} = (p_1 \dots p_\ell)^{\mathrm{T}} \qquad \boldsymbol{q} = (q_1 \dots q_\ell)^{\mathrm{T}} \\ &\mathbf{I}^0_d = \mathrm{diag}\{\boldsymbol{i}^0_d\} \qquad \mathbf{I}^0_q = \mathrm{diag}\{\boldsymbol{i}^0_q\} \qquad \boldsymbol{V}^0 = \mathrm{diag}\{\boldsymbol{v}^0\} \end{aligned}$$

and for the generic vector $\boldsymbol{x}$, upperscript 0 indicates its value in the initial operating point and $\Delta\boldsymbol{x}$ its variation with respect to such an initial value.

### 2.2. Distribution network

Steady-state operation of distribution network can be modeled by well-know DistFlow equations [33]. However, approximate linear models are more adequate for decentralized control design [34]. Adopting the constrained Jacobian-based method proposed in [35,36], the following variational model expressed with respect to an initial operating point of the network can be written

$$\Delta \boldsymbol{v}^2 = \boldsymbol{\Gamma}_P\, \Delta \boldsymbol{p} + \boldsymbol{\Gamma}_Q\, \Delta \boldsymbol{q} \tag{8}$$

where $\Delta \boldsymbol{v}^2 = \begin{pmatrix} \Delta v^2_{m_1} \dots \Delta v^2_{m_\ell} \end{pmatrix}$ and $\boldsymbol{\Gamma}_P$, $\boldsymbol{\Gamma}_Q$ are sensitivity square matrices of dimension $\ell \times \ell$. Model (8) relates the variations of the squared voltages at the DER connection nodes to the variations of the active and the reactive powers injected by each DER.

It is important to point out that the elements of the sensitivity matrices are evaluated in a given operating condition of the ADN and assuming that the line parameters of the distribution network are exactly known. Hence, operating conditions different (unknown) from the initial one as well as not exactly knowledge of the line parameters lead to uncertainty in the elements of $\boldsymbol{\Gamma}_P$ and $\boldsymbol{\Gamma}_Q$.

### 2.3. ADN

Substituting (7) for $\Delta\boldsymbol{p}$ and $\Delta\boldsymbol{q}$ in (8) and linearizing yields

$$\begin{aligned} 2\boldsymbol{V}^0 \Delta \boldsymbol{v} \;=\; & \boldsymbol{V}^0 \Delta \boldsymbol{v} \boldsymbol{\Gamma}_P \left( \boldsymbol{V}^0\, \Delta \boldsymbol{i}_d + \mathbf{I}^0_d\, \Delta \boldsymbol{v} \right) + \\ & \boldsymbol{\Gamma}_Q \left( \boldsymbol{V}^0\, \Delta \boldsymbol{i}_q + \mathbf{I}^0_q\, \Delta \boldsymbol{v} \right) \end{aligned} \tag{9}$$

By solving (9) with respect to $\Delta\boldsymbol{v}$ it is obtained

$$\Delta \boldsymbol{v} = \mathbf{A}_d\, \Delta \boldsymbol{i}_d + \mathbf{A}_q\, \Delta \boldsymbol{i}_q \tag{10}$$

where

$$\mathbf{A}_d = \mathbf{A}^{-1}\, \boldsymbol{\Gamma}_P\, \boldsymbol{V}^0 \qquad \mathbf{A}_q = \mathbf{A}^{-1}\, \boldsymbol{\Gamma}_Q\, \boldsymbol{V}^0 \tag{11}$$

with

$$\mathbf{A} = 2\, \boldsymbol{V}^0 - \boldsymbol{\Gamma}_P\, \mathbf{I}^0_d - \boldsymbol{\Gamma}_Q\, \mathbf{I}^0_q$$

Eventually, the substitution of (10) in the first of (7) yields

$$\Delta \boldsymbol{p} = \mathbf{B}_d\, \Delta \boldsymbol{i}_d + \mathbf{B}_q\, \Delta \boldsymbol{i}_q \tag{12}$$

where

$$\mathbf{B}_d = \boldsymbol{V}^0 + \mathbf{I}^0_d\, \mathbf{A}_d \qquad \mathbf{B}_q = \mathbf{I}^0_d\, \mathbf{A}_q \tag{13}$$

Combining (10) and (12) in a single matrix expression gives

$$\Delta \boldsymbol{y} = \mathbf{T}\, \Delta \boldsymbol{i} \tag{14}$$

with

$$\begin{aligned} \boldsymbol{y} &= \begin{pmatrix} \boldsymbol{y}_1 & \boldsymbol{y}_2 \dots \boldsymbol{y}_\ell \end{pmatrix}^{\mathrm{T}} = \begin{pmatrix} p_1 & v_{m_1} & p_2 & v_{m_2} & \dots & p_\ell & v_{m_\ell} \end{pmatrix}^{\mathrm{T}} \\ \boldsymbol{i} &= \begin{pmatrix} \boldsymbol{i}_1 & \boldsymbol{i}_2 \dots \boldsymbol{i}_\ell \end{pmatrix}^{\mathrm{T}} = \begin{pmatrix} i_{1d} & i_{1q} & i_{2d} & i_{2q} & \dots & i_{\ell d} & i_{\ell q} \end{pmatrix}^{\mathrm{T}} \end{aligned} \tag{15}$$

and $\mathbf{T}$ a $2\ell \times 2\ell$ matrix built using the $\ell \times \ell$ matrices $\mathbf{A}_d$, $\mathbf{A}_q$, $\mathbf{B}_d$, $\mathbf{B}_q$. In particular, for $i = 1, \dots, \ell$, the $(2i-1)$th row of $\mathbf{T}$ is obtained by alternating the elements of the $i$th row of $\mathbf{B}_d$ and $\mathbf{B}_q$, respectively; conversely, the $(2i)$th row of $\mathbf{T}$ is obtained by alternating the elements of the $i$th row of $\mathbf{A}_d$ and $\mathbf{A}_q$, respectively.

We calculate matrix $\mathbf{T}$ in model (14) assuming that null currents and powers are injected by DERs into the ADN ($\boldsymbol{i}^0 = \mathbf{0}$). Therefore

$$\boldsymbol{y} = \boldsymbol{y}^0 + \mathbf{T}\, \boldsymbol{i} \tag{16}$$

where $\boldsymbol{y}^0 = \begin{pmatrix} 0 & v^0_{m_1} & 0 & v^0_{m_1} & \dots & 0 & v^0_{m_\ell} \end{pmatrix}^{\mathrm{T}}$ represents a voltage bias.

Substituting (5) into (16) yields the following final model

$$\boldsymbol{y} = \boldsymbol{y}^0 + \mathbf{P}(s)\, \boldsymbol{u} \qquad \text{with } \mathbf{P}(s) = \mathbf{T}\, \mathbf{G}(s) \tag{17}$$

where $\mathbf{P}(s)$ is the square MIMO model of the system with $2\ell$ inputs and outputs. Moreover $\mathbf{P}(0) = \mathbf{T}\, \mathbf{G}(0) = \mathbf{T}$, see (2) and (6), where $\mathbf{P}(0)$ is the matrix that represents the steady-state ($\omega = 0$) model.

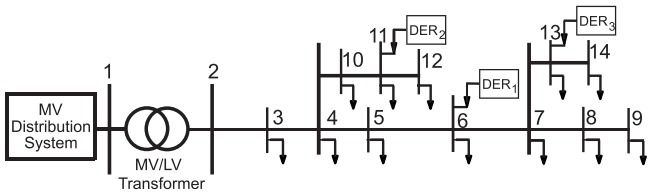


**Fig. 1.** LV ADN under study.

## 3. Proposed controllers design

In this section an independent SISO design of robust PI regulators is developed to control active power and voltage at all nodes where a DER is connected. Without loss of generality, the ADN depicted in Fig. 1 is considered. Nevertheless, applying the proposed procedure to any ADN with more feeders and DERs is straight-forward.

A 250 kVA 20/0.4 kV transformer, connected to the MV busbar (slack bus), supplies the LV substation busbar (node 2), from which a single LV feeder with three laterals departs. The electrical parameters of the lines are derived from the ones of existing LV feeders.

The rated loading of the feeder is equal to 39.0 kW and 66 kVAR of reactive power. The rated power of each DER is equal to 20 kW, whereas the reactive power can be varied in the range ±15 kVAR, with a 25 kVA VSC featuring a rectangular capability chart. All DERs are connected to the distribution system through a 25 kVA transformer and include an AC filter equipped with 4 kVAR capacitor.

The assumed operating condition of the ADN is the following: null power injections of DERs; 70% loading conditions and balanced loads; unitary per-unit values for both voltage at the slack node and ratio of the substation transformer. Based on this operating condition, matrix $\mathbf{T}$ is as follows:

$$\mathbf{T} = \begin{pmatrix} 1.0184 & 0.0070 & 0.0086 & 0.0050 & 0.0185 & 0.0071 \\ 0.0368 & 0.0140 & 0.0172 & 0.0100 & 0.0370 & 0.0142 \\ 0.0087 & 0.0051 & 1.0201 & 0.0067 & 0.0087 & 0.0051 \\ 0.0174 & 0.0101 & 0.0401 & 0.0133 & 0.0175 & 0.0102 \\ 0.0184 & 0.0070 & 0.0086 & 0.0050 & 1.0277 & 0.0083 \\ 0.0367 & 0.0140 & 0.0172 & 0.0100 & 0.0555 & 0.0167 \end{pmatrix} \tag{18}$$

Concerning the nominal parameter values of matrices $\mathbf{G}_j(s)$, they have been set equal to:

| $\tau_{1d}$ | $\tau_{1q}$ | $\tau_{11}$ | $\tau_{12}$ | $\tau_{13}$ | $\tau_{14}$ | $k_{11}$ | $k_{12}$ |
|---|---|---|---|---|---|---|---|
| 0.012 | 0.0118 | 0.014 | 0.0132 | 0.0168 | 0.0158 | $2\,10^{-5}$ | $2.2\,10^{-4}$ |
| $\tau_{2d}$ | $\tau_{2q}$ | $\tau_{21}$ | $\tau_{22}$ | $\tau_{23}$ | $\tau_{24}$ | $k_{21}$ | $k_{22}$ |
| 0.0113 | 0.0127 | 0.017 | 0.0136 | 0.0204 | 0.016 | $3\,10^{-5}$ | $3.2\,10^{-4}$ |
| $\tau_{3d}$ | $\tau_{3q}$ | $\tau_{31}$ | $\tau_{32}$ | $\tau_{33}$ | $\tau_{34}$ | $k_{31}$ | $k_{32}$ |
| 0.014 | 0.0124 | 0.016 | 0.013 | 0.0192 | 0.0168 | $2.4\,10^{-5}$ | $2.6\,10^{-4}$ |

(19)

According to model (17), matrices $\mathbf{T}$ and $\mathbf{G}(s)$ are then employed to form the nominal plant $\mathbf{P}_{nom}(s) = [P_{ij,n}(s)]$ $(i, j = 1, 2, \ldots, 6)$, where subscript $n$ stands for nominal. The system is then a square MIMO with six inputs and outputs.

Now, let us address the problem of input–output pairing which is the first step to design SISO controllers. To take this step, one of the most popular tool to quantify the system interaction is the Relative Gain Array (RGA) which is a matrix of relative gains $\mathbf{\Lambda}$ defined as [37]:

$$\mathbf{\Lambda} = \mathbf{P}(0) \otimes (\mathbf{P}(0)^{-1})^{\mathrm{T}} \tag{20}$$

The operator $\otimes$ denotes element-by-element multiplication or Schur product.

In our case Eq. (20) becomes $\mathbf{\Lambda} = \mathbf{T} \otimes (\mathbf{T}^{-1})^{\mathrm{T}}$. Hence the use of matrix $\mathbf{T}$ in (18) leads to the following RGA matrix of the considered ADN

$$\mathbf{\Lambda} = \begin{array}{c} \begin{matrix} u_{1d} & u_{1q} & & u_{2d} & u_{2q} & & u_{3d} & u_{3q} & \end{matrix} \\ \left(\begin{array}{cc|cc|cc} \mathbf{1.0184} & -0.0259 & 0 & 0.0076 & 0 & 0 & p_1 \\ -0.0184 & \mathbf{7.9681} & 0 & -1.2224 & 0 & -5.7257 & v_{m_1} \\ \hline 0 & 0.0102 & \mathbf{1.0201} & -0.0303 & 0 & 0 & p_2 \\ 0 & -1.1986 & -0.0201 & \mathbf{2.2187} & 0 & 0 & v_{m_2} \\ \hline 0 & 0.0271 & 0 & 0.073 & \mathbf{1.0277} & -0.0622 & p_3 \\ 0 & -5.7809 & 0 & 0.0208 & -0.0277 & \mathbf{6.7879} & v_{m_3} \end{array}\right) \end{array}$$

It can be observed that $\mathbf{\Lambda}$ has elements greater or about equal to one on the main diagonal while the off-diagonal elements are negative, or null, or positive and small. Hence according to the meaning of the RGA elements, the selected pairing is $(p_j - u_{jd})$ and $(v_{m_j} - u_{jq})$, $j = 1, 2, 3$. Moreover, since pairings $(p_j - u_{jd})$ are characterized by elements of matrix $\mathbf{\Lambda}$ about equal to one, any active-power control loop is decoupled from the rest of the system and can be treated as a SISO subsystem.

It is worth noting that, for any DER, there are two sources of interactions. The former is caused since two control loops (voltage and active power) exist (internal interaction). The latter is an external interaction caused by other DERs.

How it can be easily recognized form $\mathbf{\Lambda}$, the internal interaction of any DER is low, pairings $(v_{mj} - u_{jd})$ and $(p_j - u_{jq})$. On the contrary, it is present external interaction between the voltage control loops. In particular, interaction is present between $\mathrm{DER}_1$ and the others two, pairings $(v_{m1} - u_{2q})$ and $(v_{m1} - u_{3q})$; $\mathrm{DER}_2$ interacts with $\mathrm{DER}_1$, pairing $(v_{m2} - u_{1q})$; $\mathrm{DER}_3$ with $\mathrm{DER}_1$ and weakly with $\mathrm{DER}_2$, pairings $(v_{m3} - u_{1q})$ and $(v_{m3} - u_{2q})$, respectively. Hence voltage control loops are coupled.

As stated above, two control loops exist for any DER. The first regulates the active power $p_j$ to the set-point $p_{jdes}$; the second regulates $v_{mj}$ to $v_{jdes}$ and faces the problem to attenuate adverse effects of these external disturbances caused by other DERs on the regulated voltage. Concerning the set-points, $p_{jdes}$ is generally determined by the active power optimization algorithm of each DER, which is strictly dependent on the type of DER and accounts for the variable nature of renewable energy sources (such as MPPT algorithm for PV systems) and for the charging/discharging profile of the storage systems, that can account also for additional service offered to the grid. Conversely, $v_{jdes}$ is sent by the secondary voltage control, which is typically performed at area/system level so as to optimize voltage profiles along the feeders.

Let $\mathbf{C}(s) = \mathrm{diag}\{C_{1p}(s)\ C_{1v}(s)\ C_{2p}(s)\ C_{2v}(s)\ C_{3p}(s)\ C_{3v}(s)\}$ denote the diagonal control matrix, where $C_{ip}(s)$ and $C_{iv}(s)$ are the active power and voltage controllers of the $i$th DER, respectively. $\mathbf{C}(s)$ is designed to meet the following requirements:

- R1: $\lim_{t\to\infty} \boldsymbol{e} = (\boldsymbol{e}_1 \ldots \boldsymbol{e}_\ell)^{\mathrm{T}} = \mathbf{0}$ with $\boldsymbol{e}_j = (e_{jp}\ e_{jv})$ where $e_{jp} = p_{jdes} - p_j$ and $e_{jv} = v_{jdes} - v_{mj}$ are the active power and voltage regulation errors, respectively.
- R2: A desirable bandwidth pulse $\omega_{-3p}$, for the $i$th active-power control loop.
- R3: Magnitude of the closed-loop frequency response $|W_{iv}(\jmath\omega)| \leq 1\ \forall\omega \geq 0$ for the $i$th voltage control loop.
- R4: A desirable disturbance attenuation level in the $i$th voltage control loop.
- R5: Robust stability of the closed-loop system for all $\mathbf{P}(s) \in \boldsymbol{\mathcal{P}}(s)$ where $\boldsymbol{\mathcal{P}}(s) = \{\mathbf{P}(s)\}$ is the set of all possible perturbed transfer function matrices.

Based on the previous considerations, it is clear that the design of any $C_{ip}(s)$ can be developed independently from the design of all others controllers. Hence, without loss of generality, attention is focused on the design of the active power controller for $\mathrm{DER}_1$.

Using the stable nominal transfer function $P_{11,n}(s)$, the following IMC controller

$$C_{1p}^{imc}(s) = \frac{1}{P_{11}(s)\,(1 + s\lambda_{1p})} \tag{21}$$

is designed which is robust against parameter uncertainty in $P_{11}(s)$. Then, the feedback controller is given by

$$C_{1p}(s) = \frac{C_{1p}^{imc}(s)}{1 - C_{1p}^{imc}(s)\, P_{11}(s)} \tag{22}$$

which gives the following nominal closed-loop transfer function

$$W_{1p,n}(s) = \frac{1}{\lambda_{1p}} \frac{1}{(s + 1/\lambda_{1p})} \tag{23}$$

Now, from (23) it results that $\lambda_{1p}^{-1} = \omega_{-3p}$; it is then possible to fulfill requirement R2 by assigning an appropriate value to $\lambda_{1p}$. To this aim, since the bandwidth of the $i_{1d}$ current control closed-loop is equal to $1/\tau_{1d} = 1/0.012 = 83$ rad/s, see (19), it is advisable to choice $\omega_{-3p} \ll 83$ rad/s. Imposing $\omega_{-3p} = 0.5$ rad/s it obtains $\lambda_{1p} = 2$. With this choice, the settling time $t_s$ to the step response of the active-power closed-loop is about equal to 8 s ($t_s \approx 4/\omega_{-3p}$).

Employing (21) in (22) leads to the following expression

$$C_{1p}(s) = 0.0058913\, \frac{(s + 83.34)}{s}$$

which is indeed a PI controller that satisfies also requirement R1.

The same design procedure is repeated for $\text{DER}_2$ and $\text{DER}_3$ starting from the nominal transfer functions $P_{33,n}(s)$ and $P_{55,n}(s)$, respectively. Imposing $\lambda_{2p} = \lambda_{3p} = 2$, at the end of the design the following transfer functions have been obtained:

$$C_{2p}(s) = 0.0055385\, \frac{(s + 88.5)}{s} \qquad C_{3p}(s) = 0.0068105\, \frac{(s + 71.44)}{s}$$

Moving to the problem of voltage controller design, as previously evidences, each DER interacts with the two other ones. However, it is still possible to develop a design for each DER without *a priori* information of the other voltage controllers, that is an independent SISO design. It is accomplished by employing the method of the EOTF to take into account the loop interaction [26,27].

To this aim, let the following MIMO sub-system be considered

$$\mathbf{P}_v(s) = \begin{pmatrix} P_{22,n}(s) & P_{24,n}(s) & P_{26,n}(s) \\ P_{42,n}(s) & P_{44,n}(s) & P_{46,n}(s) \\ P_{62,n}(s) & P_{64,n}(s) & P_{66,n}(s) \end{pmatrix}$$

which is obtained by extracting from $\mathbf{P}_{nom}(s)$ the transfer functions corresponding to the pairings $(v_{mj} - u_{iq})$ $(i, j = 1, 2, 3)$, see matrix $\mathbf{\Lambda}$. The expression of the EOTF, $P_i^{\text{eff}}(s)$, employed in the design is given by [26]

$$P_i^{\text{eff}}(s) = \frac{P_{v,ii}(s)}{DRGA_{ii}(s)} \tag{24}$$

where $DRGA_{ii}(s)$ denotes the $i$th diagonal element of the Dynamic Relative Gain Array (DRGA) and is calculated by

$$DRGA_{ii}(s) = [\mathbf{P}_v(s) \otimes (\mathbf{P}_v(s)^{-1})^{\text{T}}]_{ii}$$

The physical meaning of the EOTF is now illustrated with reference to $\text{DER}_1$. The relation between $u_{1q}$ and $v_{m1}$, with the others two voltage control loops closed, can be expressed as follows

$$v_{m1} = \left[ P_{v,11}(s) - \bar{\mathbf{p}}^{1r}(s) \widetilde{\mathbf{C}}_{1v}(s) \left( \mathbf{I}_{2\times 2} + \bar{\mathbf{P}}_{1v}(s)\, \widetilde{\mathbf{C}}_{1v}(s) \right)^{-1} \mathbf{p}^{1c}(s) \right] u_{1q} \tag{25}$$

see Fig. 2. In (25) $\widetilde{\mathbf{C}}_{1v}(s) = \text{diag}\{C_{2v}(s)\ C_{3v}(s)\}$, $\bar{\mathbf{P}}_{1v}(s)$ denotes a transfer function matrix where both the first row and column are removed from $\mathbf{P}_v(s)$, $\mathbf{p}^{1r}(s)$ and $\mathbf{p}^{1c}(s)$ denote the first row and column vector of matrix $\mathbf{P}_v(s)$ where $P_{v,11}(s) = P_{22,n}(s)$ is discarded, respectively.

If the following approximation

$$\mathbf{H}_1(j\omega) = \bar{\mathbf{P}}_{1v}(j\omega)\, \widetilde{\mathbf{C}}_{1v}(j\omega) \left( \mathbf{I}_{2\times 2} + \bar{\mathbf{P}}_{1v}(j\omega)\, \widetilde{\mathbf{C}}_{1v}(j\omega) \right)^{-1} \simeq \mathbf{I}_{2\times 2} \tag{26}$$

holds in the frequencies range smaller than the cross-over frequency $\omega_c$, then Eq. (25) can be reasonably simplified as follows

$$v_{m1} = \left( P_{v,11}(s) - \bar{\mathbf{p}}^{1r}(s)\, \bar{\mathbf{P}}_{1v}^{-1}(s)\, \mathbf{p}^{1c} \right) u_{1q} = P_i^{\text{eff}}(s)\, u_{1q}$$

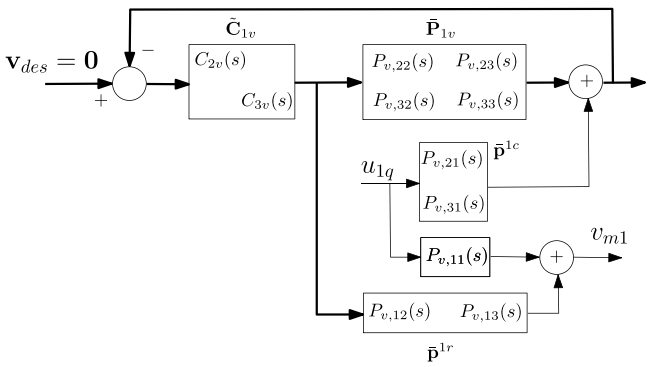


**Fig. 2.** Block scheme representation of the concept of EOTF for $\text{DER}_1$.

which does not include knowledge of other controllers.

Condition (26) is fulfilled if $C_{2v}(s)$ and $C_{3v}(s)$ include an integral action and the gain of $C_{2v}(s)$ and $C_{3v}(s)$ is greater than that of $P_{v,22}(s)$ and $P_{v,33}(s)$, respectively.

Hence, the method of the EOTF allows to independently design $C_{iv}(s)$ for model $P_i^{\text{eff}}(s)$ rather than $\mathbf{P}_v(s)$, see Fig. 3.

Let now the design of $C_{1v}(s)$ be addressed. Since $P_1^{\text{eff}}(s)$ obtained by (24) shows a complicated dynamic form, it is necessary to reduce the order of model. Any conventional reduction technique can be used for this purpose. In this section, the Hankel-norm approximation with balanced realization is applied to obtain the reduced model $P_{1,r}^{\text{eff}}(s)$.

To validate the adopted reduction technique, Fig. 4 shows that $P_{1,r}^{\text{eff}}(j\omega)$ is fairly coincident with $P_1^{\text{eff}}(j\omega)$ over the frequency range of interest.

The design of $C_{1v}(s)$ has to satisfy requirements R1, R3 and R34. Requirement R3 imposes that the step-response of the voltage control loop presents null overshoot. To fulfill R3 we use the following expression [38]

$$m_\varphi \geq 180 - 2\left(\frac{180}{\pi}\right) \cos^{-1}\left(\frac{0.5}{\bar{W}}\right)$$

which gives a relationship between the phase-margin $m_\varphi$ and the circle of magnitude constant $\bar{W}$ of the closed-loop transfer function in the Nichols chart. By imposing $\bar{W} = 1$ (no overshoot) it results $m_\varphi \geq 60°$.

As concerns requirement R4, let

$$M_{1v}(s) = \frac{1}{1 + C_{1v}(s)\, P_{11,r}^{\text{eff}}(s)} \tag{27}$$

define the transfer function from the disturbance $d_1$ to the system output $v_{m1}$, i.e., $V_{m1}(s) = M_{1v}(s)\, D_1(s)$, see Fig. 3. Requirement R4 is then formulated as the following specification

$$|M_{1v}(j\omega)| \leq |DAL(j\omega)| \qquad \forall \omega \in \Omega_v = [0 \quad \omega_{-3v}] \tag{28}$$

where

$$DAL(j\omega) = \frac{j\omega}{4 + j\omega} \tag{29}$$

is the considered disturbance attenuation level (DAL) and $\omega_{-3,v}$ is the bandwidth pulse of the closed-loop system. The frequency bound $\Omega_v$ in (28) has been selected to guarantee the desired DAL in the frequencies range of interest.

The design of $C_{1v}(s)$ is then developed using the package *pidTuner* with option *"design domain": frequency* of the Control Toolbox in Matlab software. In particular, it is set $m_\varphi = 84°$ and $\omega_{-3v} = 10 \ll 1/\tau_{1q} = 84.7$ rad/s. Having imposed $m_\varphi = 84°$, it results that $\omega_c$ is slightly smaller than $\omega_{-3v}$.

Using the plot of $M_{1,v}(j\omega)$ and $W_{1v}(j\omega)$ drawn in the package *pidTuner* during the design phase, it is possible to find the expression of $C_{1v}(s)$ that satisfies requirements R1, R3 and R4. It is obtained:

$$C_{1v}(s) = 2.241 \left(1 + \frac{1}{3.769\, 10^{-4}\, s}\right)$$

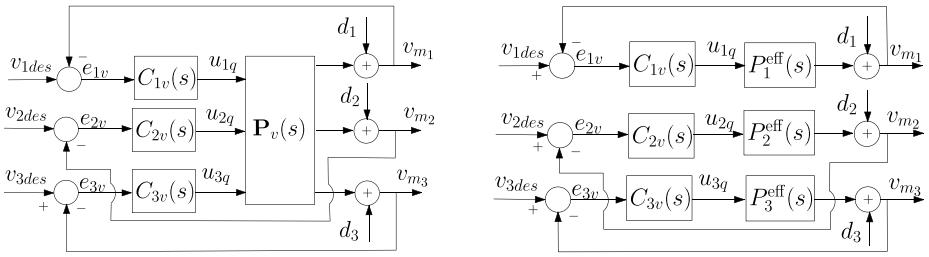


**Fig. 3.** Multi-loop system (left) and equivalent SISO systems with effective open-loop transfer function (right).

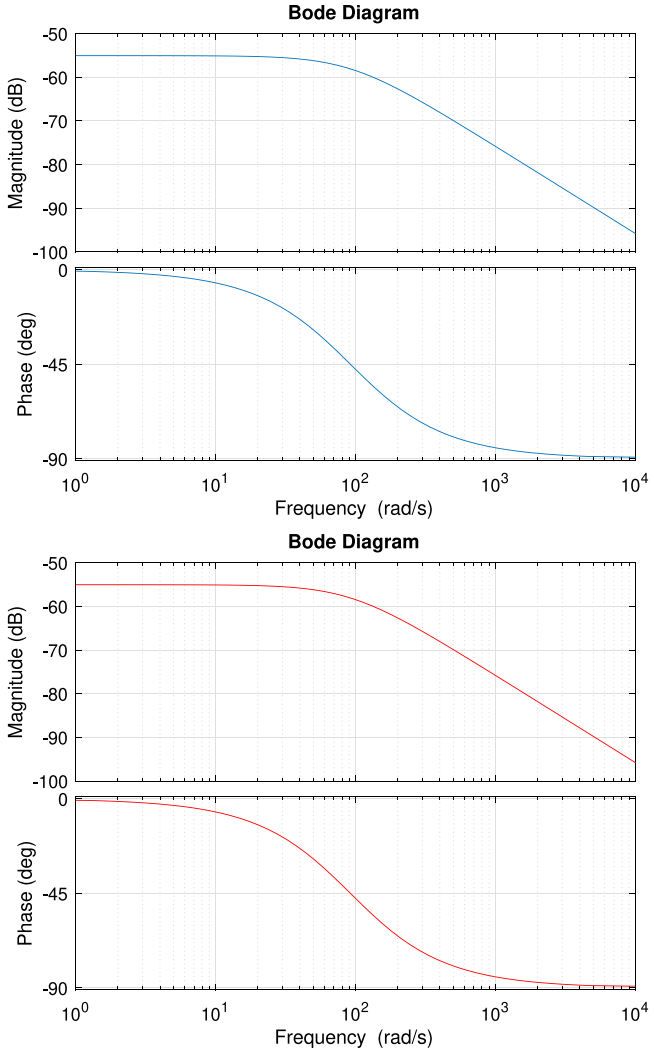


**Fig. 4.** Bode diagram of $P_1^{\text{eff}}(\jmath\omega)$ (blue) and $P_{1,r}^{\text{eff}}(\jmath\omega)$ (red) over the frequencies range of interest.

which is a PI controller. Concerning requirements R3 and R4, Figs. 5 and 6 graphically show the Bode diagram of $|W_{1v,n}(\jmath\omega)|$ and the analysis of the disturbance rejection at the output of the reduced effective open-loop transfer function $P_{11,r}^{\text{eff}}(s)$, respectively. It can be concluded that requirements R3 and R4 are satisfied.

The same phase margin and bandwidth pulse are imposed in the design of $C_{2v}(s)$ and $C_{3v}(s)$. Hence, repeating the same design procedure, from the package *pidTuner* it is obtained

$$C_{2v}(s) = 4.084\left(1+\frac{1}{2.342\,10^{-3}\,s}\right)$$
$$C_{3v}(s) = 5.754\left(1+\frac{1}{1.428\,10^{-3}\,s}\right)$$

From the analysis of Figs. 7 and 8 it is possible to state that requirement R3 is satisfied also for $\text{DER}_2$ and $\text{DER}_3$. Moreover, considering the same disturbance attenuation level (29) and the same interval $\Omega_v$, from the analysis of Figs. 9 and 10 it is possible to conclude that requirement R4 is fulfilled too.

Once $\mathbf{C}(s)$ is designed, it is interesting to validate the approximation expressed by condition (26). To this aim, Fig. 11 reports the Bode diagram of $\mathbf{H}_1(\jmath\omega)$. Since the cross-over frequency is about equal to 7 rad/s, it can be concluded that the approximation in (26) can be reasonably considered valid. Same considerations can be repeated for $\text{DER}_2$ and $\text{DER}_3$. In general, it is important to point out that the smaller the frequency $\omega$ with respect to $\omega_c$, the better the approximation $\mathbf{H}_i(\jmath\omega) \simeq \mathbf{I}_{5\times5}$.

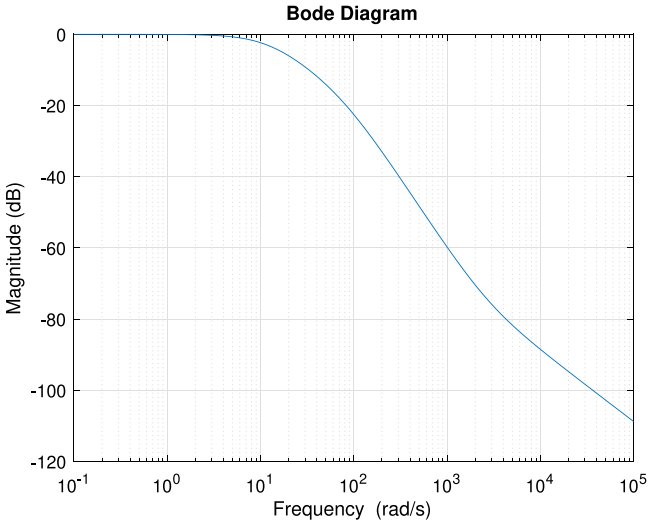


**Fig. 5.** Bode diagram of $|W_{1v,n}(j\omega)|$.

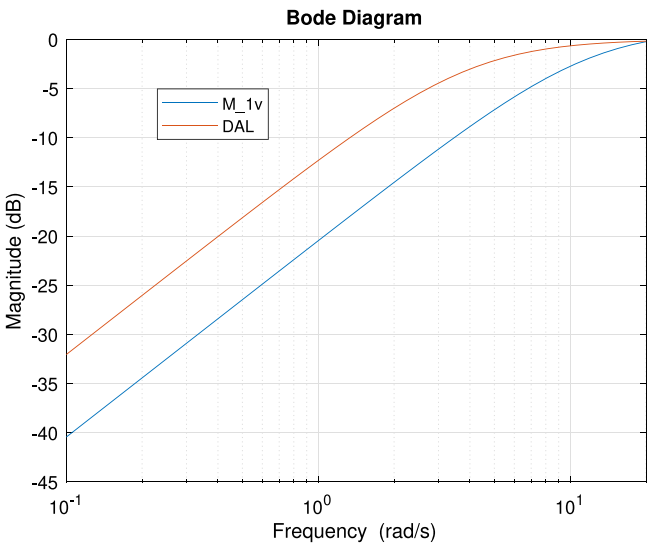


**Fig. 6.** Sensitivity analysis for $\mathrm{DER}_1$ in the nominal case.

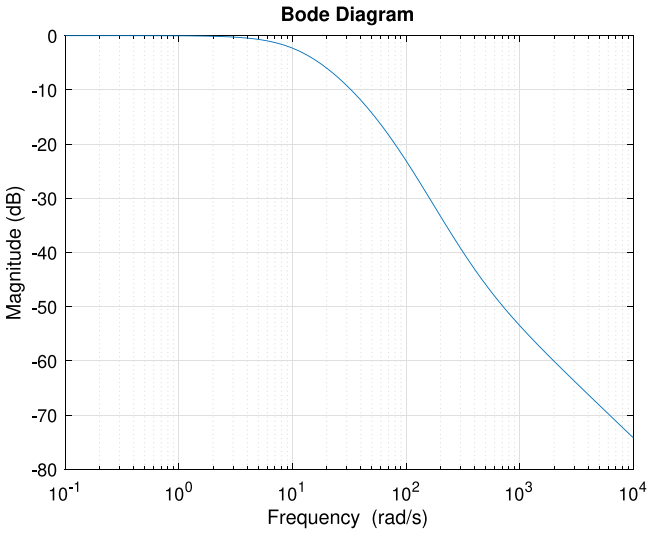


**Fig. 7.** Bode diagram of $|W_{2v,n}(j\omega)|$.

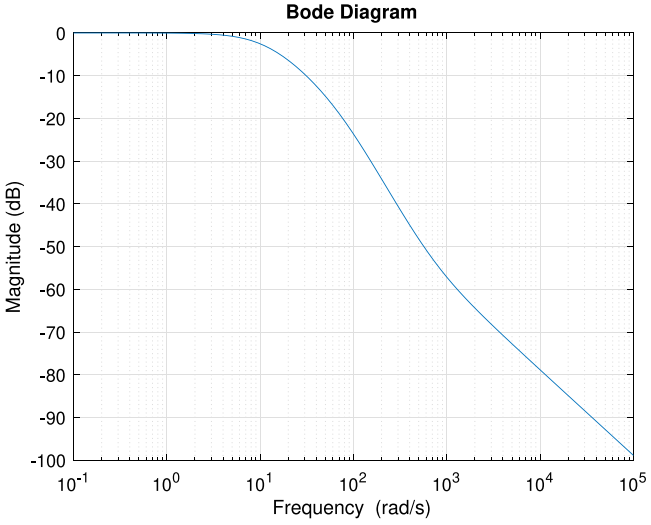


**Fig. 8.** Bode diagram of $|W_{3v,n}(j\omega)|$.

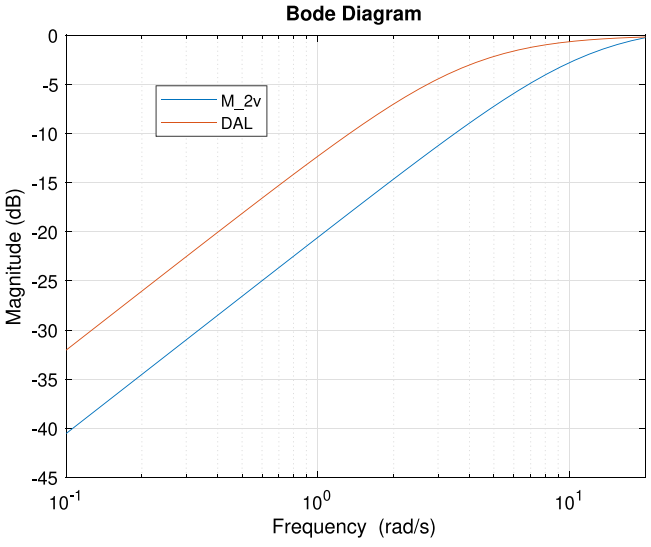


**Fig. 9.** Sensitivity analysis for $\mathrm{DER}_2$ in the nominal case.

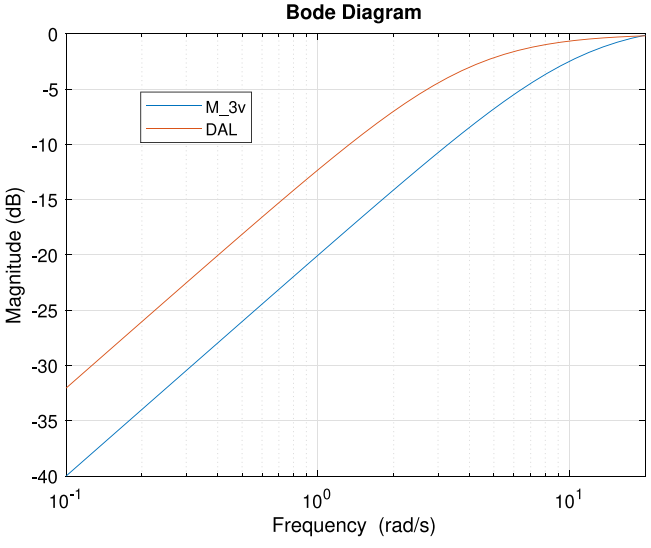


**Fig. 10.** Sensitivity analysis for $\mathrm{DER}_3$ in the nominal case.

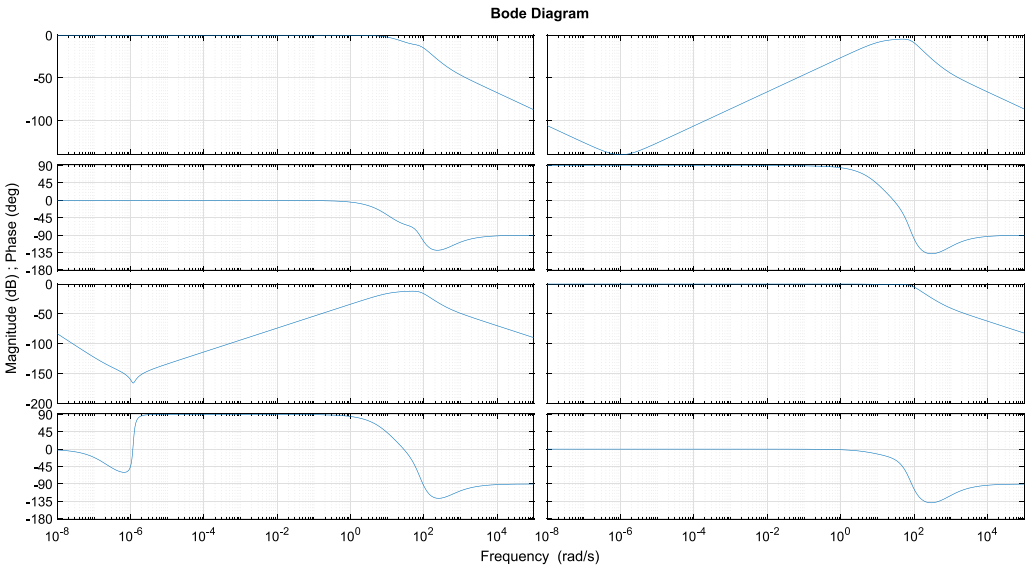


**Fig. 11.** Bode diagram of $\mathbf{H}_1(j\omega)$.

To complete the illustration of the design procedure, it is necessary to verify requirement R5. To this scope it is assumed that matrices $\mathbf{T}$ and $\mathbf{G}(s)$ in model (17) may deviate from their nominal values. As concerns matrix $\mathbf{T}$, it is worth reminding that, by assuming a given (nominal) operating condition of the ADN and the exact knowledge of the line parameters, a couple of sensitivity matrices $\mathbf{\Gamma}_P$ and $\mathbf{\Gamma}_Q$ is obtained, and consequently, a matrix $\mathbf{T}$. Hence, for each operating condition different from the nominal one, a matrix $\mathbf{T}$ different from that reported in (18) is determined. Hereafter, the following variations are considered: slack voltage from 0.95 to 1.05 p.u.; loads from 0.3 to 1.2 of their rated values; DER active powers from 0 to 20 kW and reactive powers in the range ±15 kVAR. Moreover, it is assumed that parameters $\tau_{di}$ and $\tau_{qi}$ of matrices $\mathbf{G}_j(s)$ may deviate up to ±20% from their nominal values listed in (19). Conversely, it is assumed that parameters $\tau_{ji}$ ($j = 1, 2, 3$, $i = 1, ..4$), $k_{j1}$ and $k_{j2}$ are not affected by uncertainty. This assumption is acceptable because $\mathbf{G}_j(0) = \mathbf{I}$ and the values of $k_{j1}$ and $k_{j2}$ are quite small. By combining all the considered sources of uncertainty, a family of transfer functions $\boldsymbol{\mathcal{P}}(s)$ is obtained, including 900 different matrices $\mathbf{P}(s) = \mathbf{TG}(s)$.

For any plant $\mathbf{P}(s) \in \boldsymbol{\mathcal{P}}(s)$, the following MIMO closed-loop matrix is built

$$\mathbf{W}(s) = \left(\mathbf{I} + \mathbf{P}(s)\,\mathbf{C}(s)\right)^{-1} \mathbf{P}(s)\,\mathbf{C}(s)$$

and the corresponding largest pole computed. At the end of the procedure a set of 900 poles is obtained whose plot is depicted in Fig. 12. One can see that the requirement R5 is fulfilled.

Furthermore, to complete the analysis in presence of perturbed plants, it is examined if requirements R2, R3 and R4 are fulfilled in a robust sense. As concerns requirement R2, for each of the 900 perturbed plants $\mathbf{P}(s)$, the transfer functions $P_{11}(s)$ and $C_{1p}(s)$ are employed to form the closed-loop active power transfer functions $W_{1p}(s)$ for $\text{DER}_1$. Obviously, in forming $W_{1p}(s)$ there will be no cancellation between $C_{1p}(s)$ and any of the 900 $P_{11}(s)$, except in the case of $P_{11,n}(s)$. Afterwards, it is determined the worst case among the 900 $W_{1p}(s)$ and reported in Fig. 13. The same procedure is developed for $\text{DER}_2$ and $\text{DER}_3$ starting from $P_{33}(s)$, $C_{2p}(s)$ and $P_{55}(s)$, $C_{3p}(s)$, respectively, and the corresponding results reported in Fig. 14 and Fig. 15, respectively. From the analysis of these figures it is possible to affirm that requirement R2 is robustly fulfilled.

Concerning the robust analysis in the case of requirements R3 and R4, a matrix $\mathbf{P}_v(s)$ has been built for each of the 900 perturbed plant $\mathbf{P}(s)$. Subsequently, for each $\mathbf{P}_v(s)$, the reduced EOTFs $P^{\text{eff}}_{ii,r}(s)$ have been determined as in (24), leading to 900 closed-loop transfer functions $W_{iv}(j\omega)$ and 900 transfer functions $M_{iv}(j\omega)$ for each DER. Fig. 16 shows the Bode diagram of $|W_{iv}(j\omega)|$ in the worst case, while Fig. 17 depicts the analysis of the disturbance rejection in the worst case, over the frequency range of interest. From the analysis of these figures it can be concluded that also requirements R3 and R4 are achieved in a robust sense.

Finally, the following discussion evidences some aspects of the proposed design. First, the design of $C_{iv}(s)$ uses the reduced model $P_{ir}^{eff}(s)$ of the EOTF $P_i^{eff}(s)$. If $P_i^{eff}(s)$ presents $h$ unstable poles, the order of $P_{i,r}^{eff}(s)$ must be at least equal to $h$. Therefore, the order of $P_{i,r}^{eff}(s)$ increases with respect to the case of all stable poles of $P_i^{eff}(s)$. Consequently, the complexity of the controller $C_{iv}(s)$ increases and its implementation may result difficult. However in these cases, $C_{iv}(s)$ can always be approximated by a PI/PID based on the coefficient matching method starting from the Maclaurin series expansion of $C_{iv}(s)$, see e.g. [39].

Second, the validity of the approximation (26) must be verified *a posteriori*, that is once that all $C_{iv}(s)$ have been designed and repeated for each DER. If the approximation (26) should not be fulfilled, it is necessary to repeat the design by slightly increasing the gain of all $C_{iv}(s)$ till the approximation (26) is fulfilled.

Third, if there is no solution for the assigned requirements, these latter ones should be redefined by the designer. Hence, the proposed design procedure is repeated till the assigned requirements are fulfilled.

Fourth, in the case of installation of a new DER or structural changes of the network topology, it is necessary to develop a new design. The updated gains are sent by the DSO to the local controllers by a low-capacity low-cost one-way communication, f.i. based on standard wireless mobile telecommunications technology. However, these circumstances are rare and known in advance since they require a planning activity by the DSO. On the contrary, during operation, if a DER is switched off, no action is required (see next Section *Case2* first scenario).

## 4. Case studies and validation

The proposed control is tested for selected scenarios of two different ADNs. In detail, *Case1* considers as test system the ADN shown in Fig. 1 that was used in Section 3 to illustrate the application of the proposed design procedure. *Case2* and *Case3* consider a larger LV ADN with three feeders, multiple sub-feeders, 36 nodes and nine DERs,

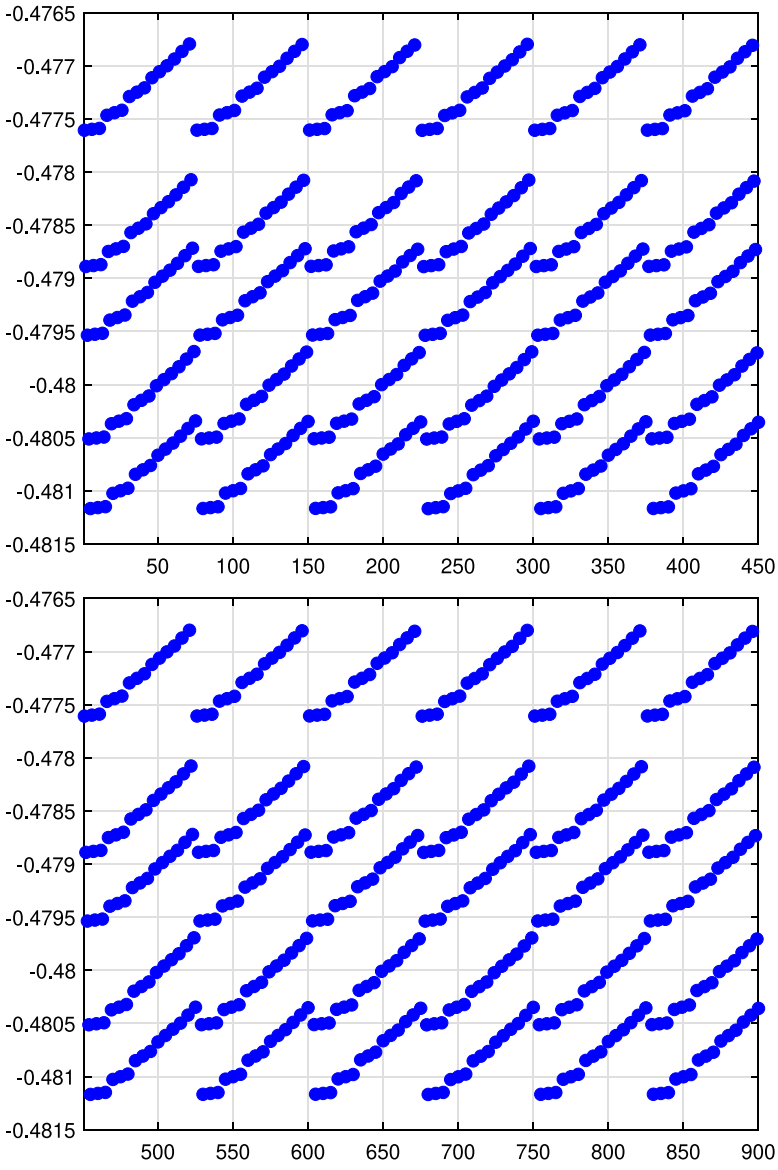


**Fig. 12.** Plot of the set formed by the largest pole of any of the 900 matrices $\mathbf{W}(s)$. First set (top) and second set (buttom).

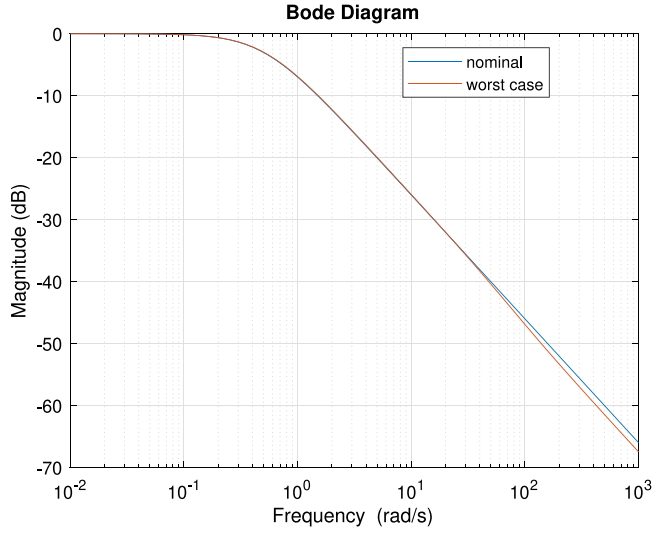


**Fig. 13.** Bode diagram of $|W_{1p,n}(j\omega)|$ and $|W_{1p}(j\omega)|$ in the worst case.

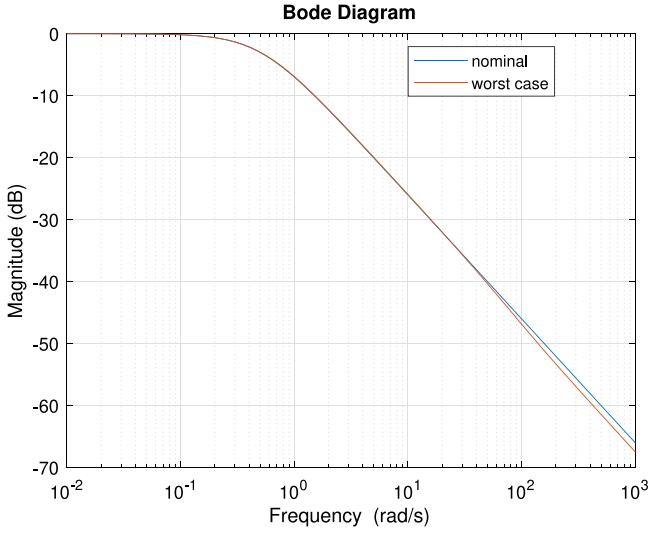


**Fig. 14.** Bode diagram of $|W_{2p,n}(j\omega)|$ and $|W_{2p}(j\omega)|$ in the worst case.

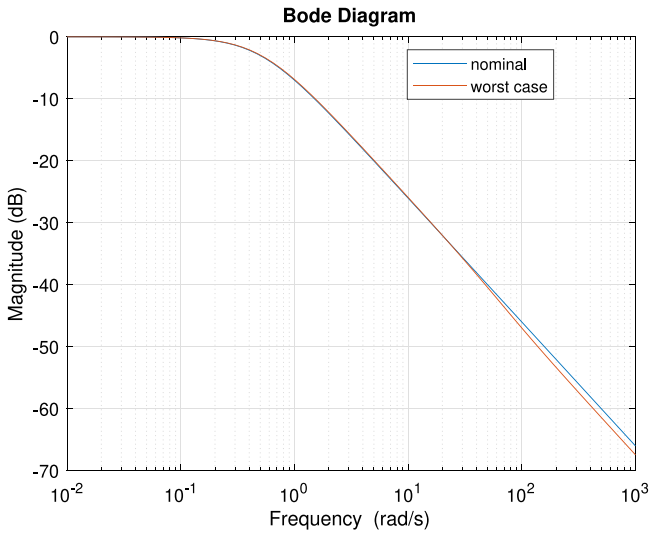


**Fig. 15.** Bode diagram of $|W_{3p,n}(j\omega)|$ and $|W_{3p}(j\omega)|$ in the worst case.

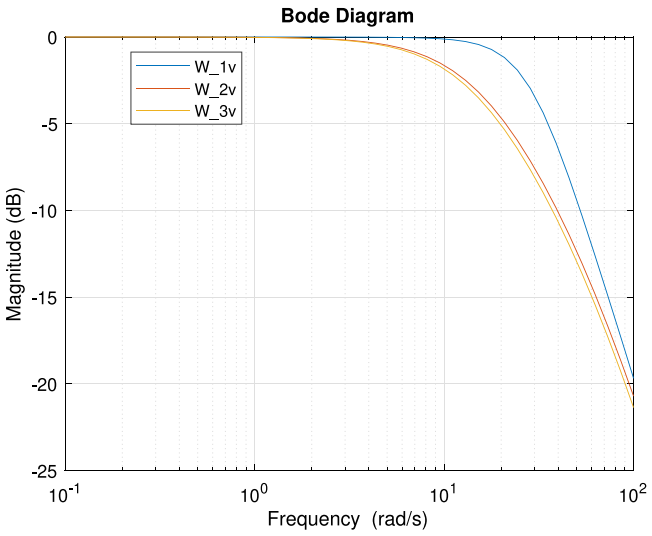


**Fig. 16.** Bode diagrams of $|W_{1v}(j\omega)|$, $|W_{2v}(j\omega)|$ and $|W_{3v}(j\omega)|$ in the worst case.

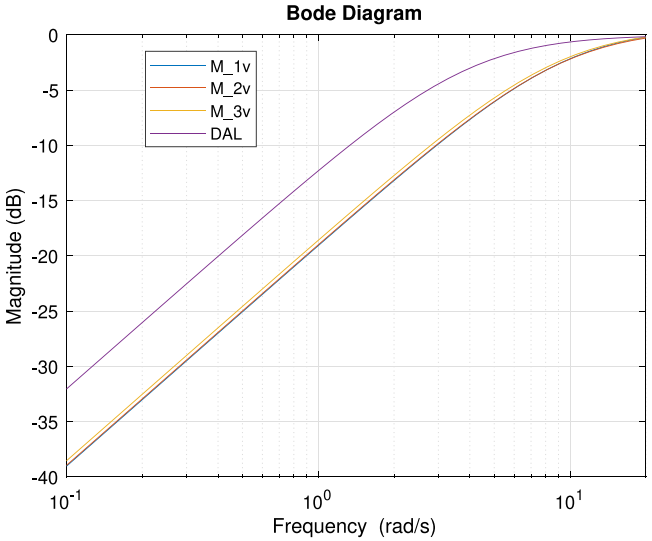


**Fig. 17.** Sensitivity analysis: Bode diagram of $|M_{1v}(j\omega)|$, $|M_{2v}(j\omega)|$ and $|M_{3v}(j\omega)|$ in the worst case.

respectively all PV systems in *Case2* and four PV systems and five Wind Turbine Generators (WTGs) in *Case3*. In all the cases each DER is equipped with a 20 kW–25 kVA VSC interfacing to the LV network; however, the various VSCs differ for their dynamics and consequently present different parameters of the transfer functions in (2). All the simulations have been developed in PSCAD/EMTDC environment [40]. Concerning the DERs, the models available in the software library of the PSCAD are used for the DC sources and for the PLLs, whereas the current-controlled VSCs are simulated using the equivalent dynamic average-value model and the current controllers described in [41]. Quantities in *per unit* are expressed on a 25 kVA power basis.

*Case1* — Five scenarios are simulated and the obtained results are hereafter reported and discussed, with the aim of giving evidence of the fulfillment of the requirements R1–R5 by the design procedure according to Section 3. The expression of the six regulators $C_{ip}(s)$ and $C_{iv}(s)$, $i = 1,2,3$ are reported in Section 3. The starting operating condition of the ADN assumes: slack voltage equal to 1.0 p.u., nodal loads equal to 70% of their rated values, $v_{ides} = 1$ and solar irradiance equal to 500 W/m$^2$. Then, all the simulated operating conditions differ from the nominal ones.

In the first scenario, $p_{1des}$ is subject to a step variation from 0.3 to 0.4 p.u. at $t = 40$ s. The aim is to analyze the interaction among the active power control loops of the three DERs. From Fig. 18 it is apparent that interactions are not detectable, as expected from the RGA analysis conducted in Section 3. The response of the active power control loop of DER$_1$ is smooth, with zero steady-state error and with a settling time coherent with the assigned bandwidth pulse equal to 0.5 rad/s (see requirements R1 and R2 in the previous paragraph).

In the second scenario, $v_{3des}$ is subject to a step variation from 1.00 to 1.002 p.u. at $t = 40$ s. Fig. 19 reports the response of the three voltage control loops. It is apparent that, despite the mutual interactions among the voltage control loops, the regulators guarantee system stability, whereas at the same time $C_{2v}(s)$ and $C_{3v}(s)$ effectively counteracts the effects due to the regulation action of $C_{1v}(s)$. Concerning the response of the voltage control loop of DER$_1$, it is smooth, with zero steady-state error and null overshoot, thus confirming that requirements R1 and R3 have been fulfilled. The mutual influence of DER$_3$ on the other DERs is contained: the voltage variations of DER$_1$ and DER$_2$ are limited within about 0.0005 p.u. and 0.00025 p.u., respectively. The results of this simulation validate the goodness of the proposed design procedure developed for the reduced EOTF.

The third scenario reproduces the worst case studied in Section 3 and reported in Fig. 16. In details, all loads are increased up to 120% of

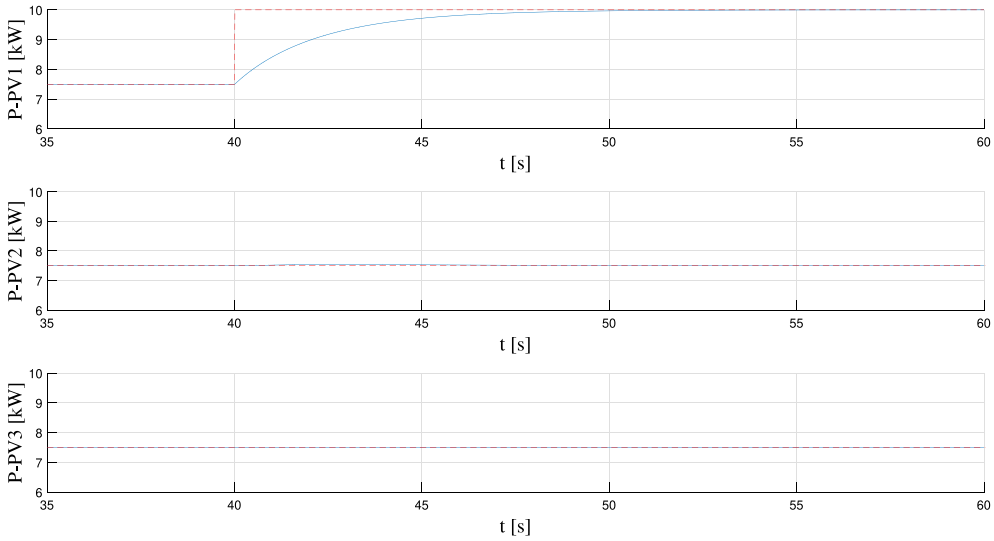


**Fig. 18.** *Case1: first scenario.* Time evolution of $p_1$, $p_2$ and $p_3$ in response to a step change of $p_{1des}$ from 0.3 to 0.4 p.u. at $t = 40$ s.

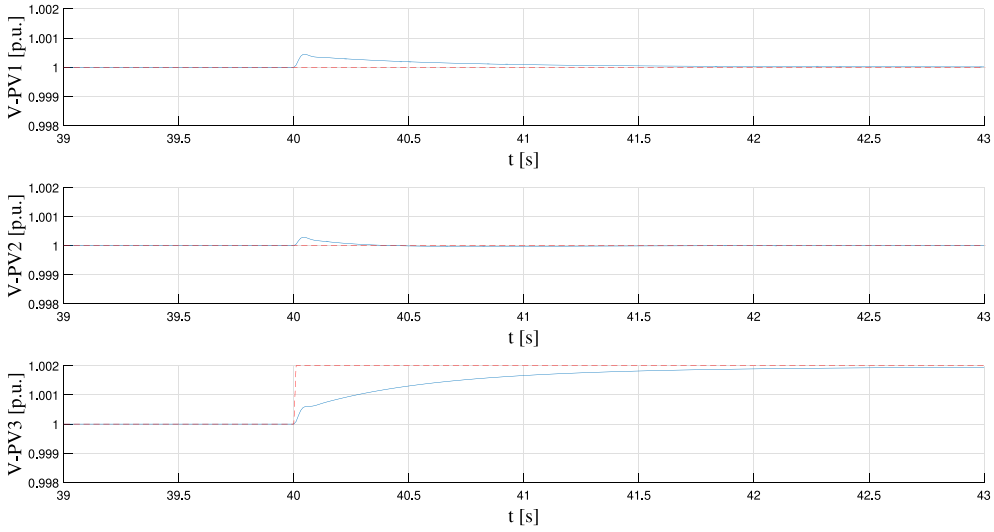


**Fig. 19.** *Case1: second scenario.* Time evolution of $v_{m1}$, $v_{m2}$ and $v_{m3}$ in response to a step change of $v_{3des}$ from 1.00 to 1.002 p.u. at $t = 40$ s.

their rated values, the slack bus voltage is equal to 0.95 p.u., the DER active power set-points are equal to 0.1 p.u. and $v_{1des} = 0.9186$ p.u., $v_{2des} = 0.9279$ p.u., $v_{3des}0.912$ p.u. At $t = 40$ s $v_{3des}$ is subject to a step increase from 0.912 to 0.914 p.u. Also in this new operating condition $v_{m1}$, $v_{m2}$ and $v_{m3}$ exhibit a smooth stable time evolution, see Fig. 20, similar to the one shown in the second scenario. This confirms that the PI regulators are able to respond in the same way to the effects caused by mutual interactions even in extremely different operating conditions.

In the fourth scenario a measurement disturbance $d_1$ represented by a sinusoidal signal of amplitude $1.0\,10^{-3}$ p.u. and pulse of 5 rad/s is added to the output of the voltage control loop of $\text{DER}_1$. The choice of the pulse equal to 5 rad/s is significant from the disturbance rejection point of view since it is near the bandwidth pulse of the voltage control loop ($\omega_{1v} = 10$ rad/s). From Fig. 21 it can be observed that $v_{m1}$ is sinusoidal with a peak value about equal to $2.98\,10^{-4}$ p.u. Consequently

$$|M_1(j5)| = \frac{2.98\,10^{-4}}{1.0\,10^{-3}} = 0.298 < |DAL(j5)| = 0.7809$$

Hence, the desired level of disturbance attenuation expressed by (28) is robustly guaranteed as required by the control objective R4.

The fifth scenario simulates a variation of the slack voltage from 1 to 1.001 p.u. at $t = 40$ s. As shown in Fig. 22 the controllers show a quite similar quick reaction; voltages recover the imposed set-point in few tenths of a second after the slack voltage variation is applied. It is also evident that the response of each voltage control loop does not affect the response of the two other ones.

*Case2* — With reference to the larger ADN shown in Fig. 23, the proposed procedure has been applied to design the PI regulators for both active power and voltage of the 9 DERs of the same type as the one of *Case1*. The results for two scenarios are reported hereafter.

The first scenario considers a voltage deviation of the slack bus from 1.0 to 1.005 p.u. at $t = 40$ s and the disconnection of $\text{DER}_5$ at $t = 50$ s. As reported in Fig. 24, voltages $v_{m4}$, $v_{m6}$ and $v_{m7}$ increase in response to the slack voltage variation while decrease when $\text{DER}_5$ is disconnected. All voltages quickly recover to their voltage set-points, whereas $v_{m4}$ differs from $v_{4des}$ due to the saturation of $u_{4q}$ between $t = 40$ s and $t = 50$ s.

In the second scenario the value of the lines resistance is increased by a 20% and a 3.96 kVAr load is suddenly connected at bus 7 at $t = 50$ s. From Fig. 25, it is apparent that voltages $v_{m1}$, $v_{m2}$ and $v_{m3}$ robustly reject the undesired effects due to uncertainty in the lines resistance

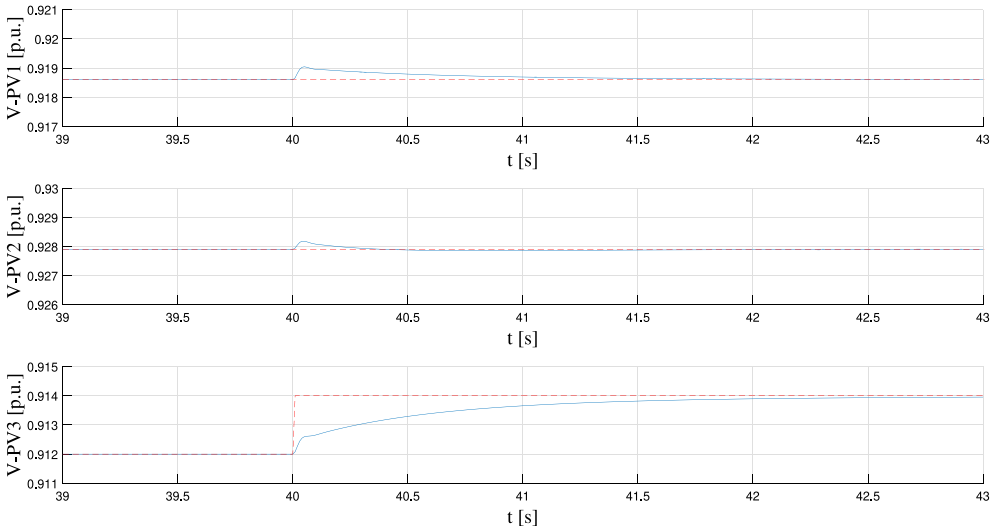


**Fig. 20.** *Case1: third scenario.* Time evolution of $v_{m1}$, $v_{m2}$ and $v_{m3}$ in response to an increase of all loads by 20% (worst case) and to a change of $v_{3des}$ from 0.912 to 0.914 p.u. at $t = 40$ s.

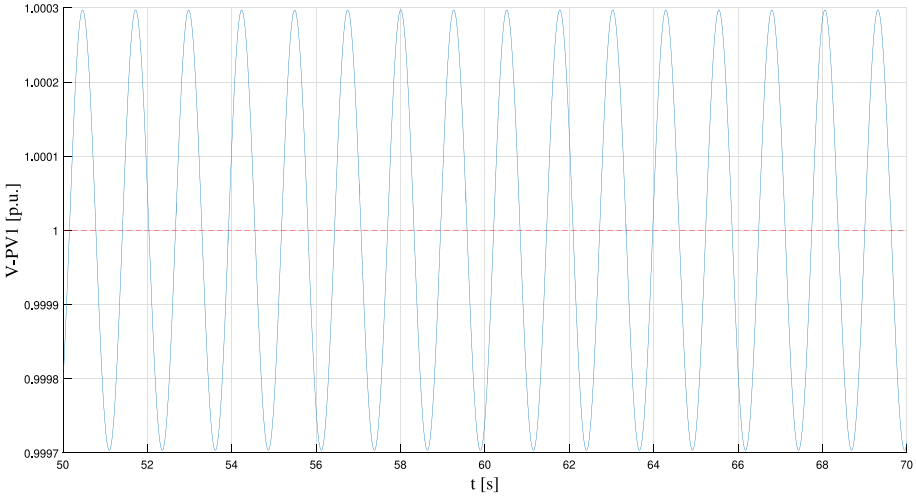


**Fig. 21.** *Case1: fourth scenario.* Time evolution of $v_{m1}$ in response to a voltage disturbance $d_1 = 1.0\,10^{-3}\,\sin(5\,t)$ p.u applied at $t = 40$ s in the voltage control loop of DER1.

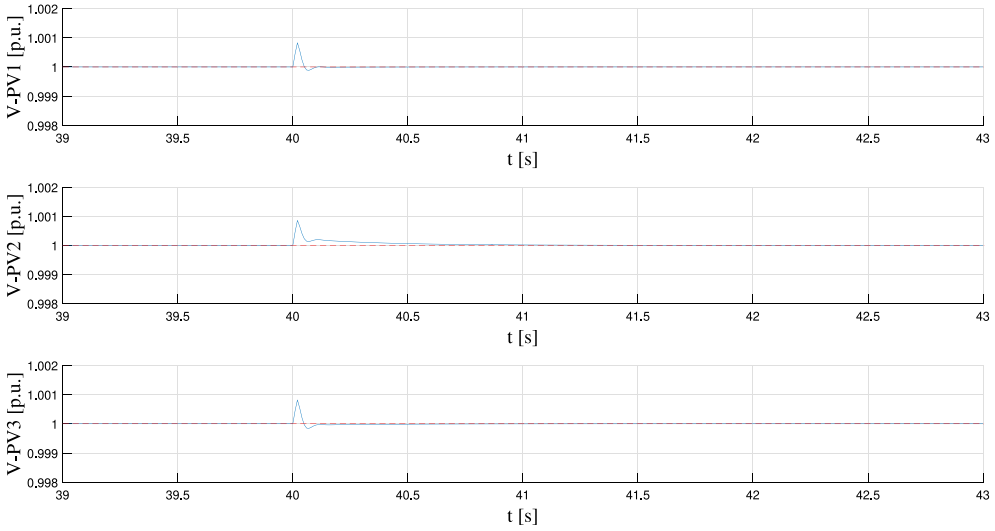


**Fig. 22.** *Case1: fifth scenario.* Time evolution of $v_{m1}$, $v_{m2}$ and $v_{m3}$ in response to variation of the slack voltage from 1 to 1.001 p.u. at $t = 40$ s.

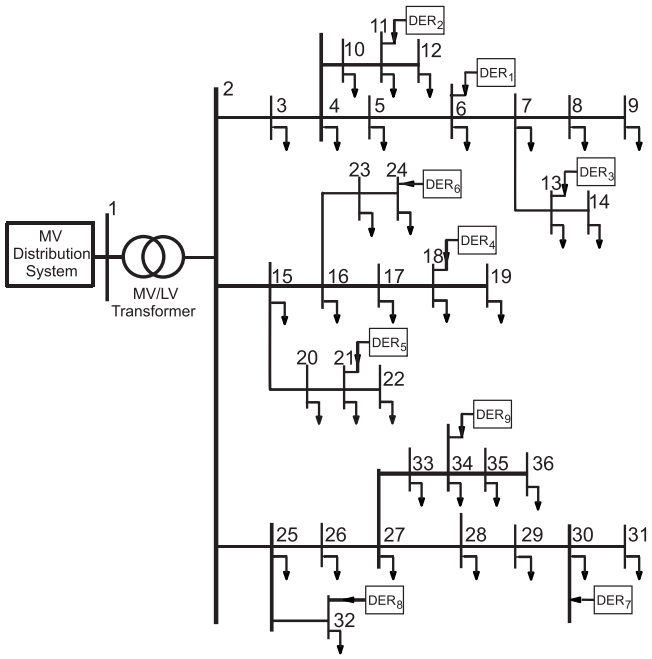


**Fig. 23.** LV ADN with 36 nodes and 9 DERs.

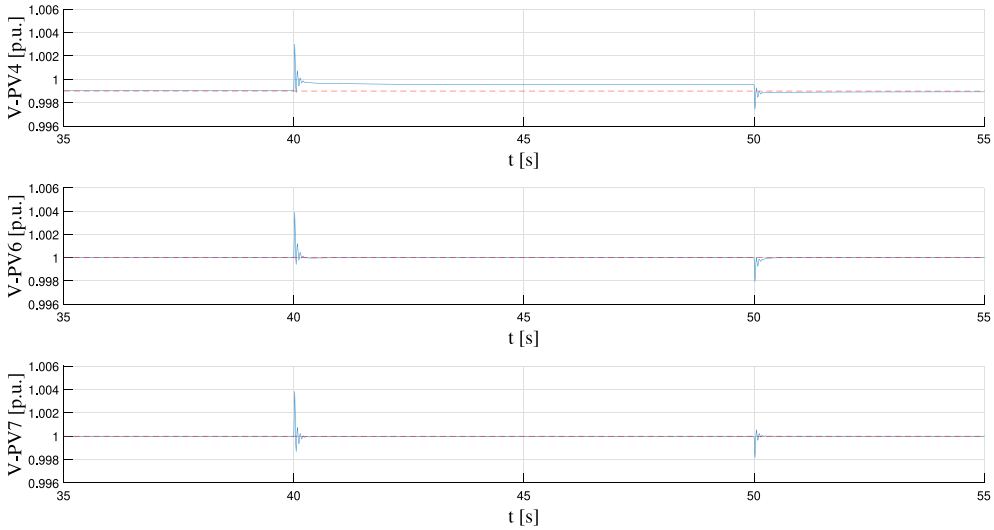


**Fig. 24.** *Case2: first scenario.* Time evolution of voltages $v_{m4}$, $v_{m6}$ and $v_{m7}$ in response to a slack voltage variation from 1.0 to 1.005 p.u. at $t = 40$ s followed by the disconnection of $DER_5$ at $t = 50$ s.

and to load insertion. The voltages recover the desired set-points in about 0.3 s.

*Case3* — The aim of the simulation results presented hereafter is to give evidence of the applicability of the proposed design procedure to DERs with different renewable energy conversion systems and to analyze the performance of the control systems in response to large voltage perturbations. In details, always with reference to the larger ADN shown in Fig. 23, DERs #1, 4, 5, 7 are PV systems whilst DERs #2, 3, 6, 8, 9 are 20 kW WTGs. Since all the DERs are interfaced to the ADN by the same type of VSC, the same PI regulators for both active power and voltage are adopted for each DER as the ones of *Case2*. To give a large voltage perturbation, at node #31 a 50 kW–25 kVAr load is connected at $t = 40$ s and then disconnected at $t = 50$ s.

To give evidence of the effective response of the voltage controls, Fig. 26 reports the voltages $v_{m7}$, $v_{m8}$ and $v_{m9}$ which are related to the DERs on the third feeder where the load variation takes place. Due to the large load connection, the DERs reactive powers saturate and are not large enough to keep the voltages to the unitary set-point. After the load disconnection, the voltages recover the starting unitary value. The voltage variations are fast and smooth also in this case. Finally, it is important to underline that all the reported simulations have been run considering the ADNs in operating conditions different from the nominal one, in which the ADN linear models have been calculated and the PI regulators designed. Then, it can be stated that requirement R5 is always fulfilled, according to the analysis of robust stability presented in Section 3.

## 5. Conclusions

In this paper, a local PI robust control has been presented for voltage and active power of converter-based DERs using the $dq$ current components. A MIMO model has been proposed to represent the ADN. Each

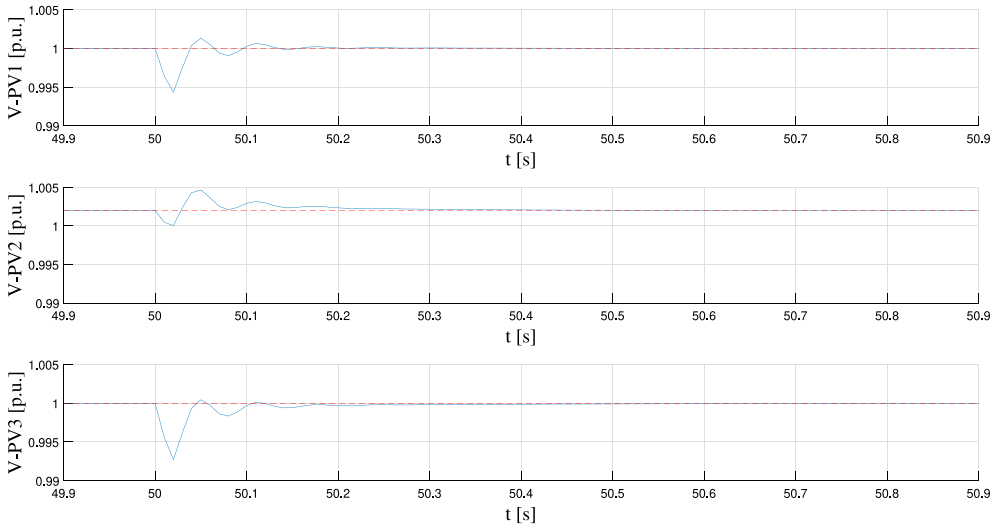


**Fig. 25.** *Case2: second scenario.* Time evolution of voltages $v_{m1}$, $v_{m2}$ and $v_{m3}$ in presence of increased line resistances by 20% and in response to a 3.96 kVAr load insertion at bus 7 at $t = 50$ s.

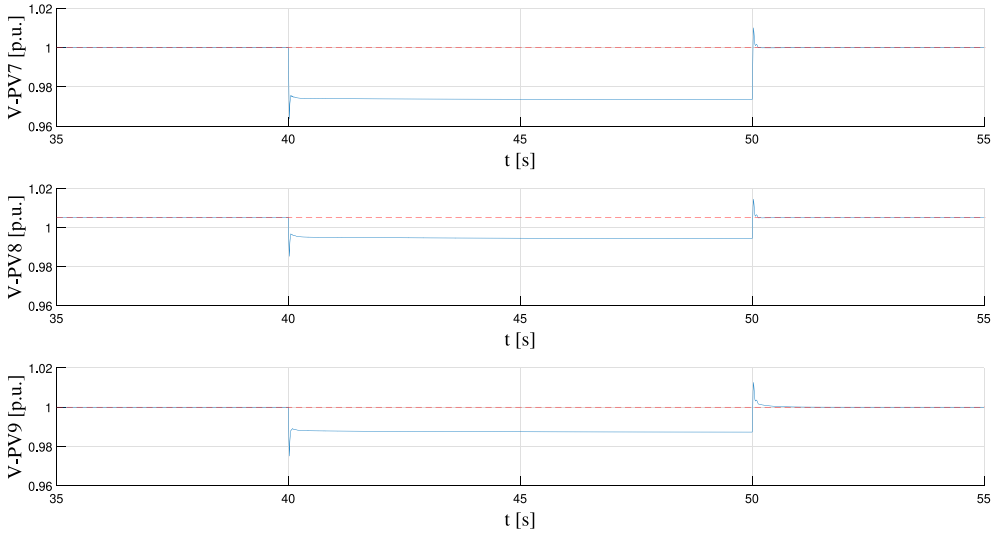


**Fig. 26.** *Case3.* Time evolution of voltages $v_{m7}$, $v_{m8}$ and $v_{m9}$ in response to a large load connection at $t = 40$ s and disconnection at $t = 50$ s.

DER is equipped with two PI regulators independently designed using a reduced model which is obtained by applying the method of the EOTF. The design guarantees robust performance and stability for a large set of perturbed plants despite the presence of interactions between DERs. Finally, results of numerical simulation studies are presented to validate the controller performance in the case of two different ADNs under different realistic scenarios. A future development of our research will concern the use of a consensus-based model predictive control approach to handle the presence of saturation and to optimally design the control laws.

## CRediT authorship contribution statement

**Giuseppe Fusco:** Conceived and designed the analysis, Contributed data or analysis tools, Performed the analysis, Wrote the paper. **Mario Russo:** Conceived and designed the analysis, Contributed data or analysis tools, Performed the analysis, Wrote the paper. **Giovanni Mercurio Casolino:** Collected the data, Contributed data or analysis tools, Performed the analysis, Wrote the paper.

## Declaration of competing interest

The authors declare the following financial interests/personal relationships which may be considered as potential competing interests: Mario Russo reports financial support was provided by Government of Italy Ministry of Education University and Research.

## Data availability

Data will be made available on request.

## Acknowledgments

The research has been funded by the Project: Ecosistema dell'innovazione - Rome Technopole, financed by EU in NextGenerationEU plan through MUR Decree n. 1051 23.06.2022 - CUP H33C22000420001

## References


[1] Eltigani D, Masri S. Challenges of integrating renewable energy sources to smart grids: A review. Renew Sustain Energy Rev 2015;52:770–80. http://dx.doi.org/10.1016/j.rser.2015.07.140.

[2] Sun H, Guo Q, Qi J, Ajjarapu V, Bravo R, Chow J, et al. Review of challenges and research opportunities for voltage control in smart grids. IEEE Trans Power Syst 2019;34(4):2790–801. http://dx.doi.org/10.1109/TPWRS.2019.2897948.

[3] Mahmoud K, Lehtonen M. Three-level control strategy for minimizing voltage deviation and flicker in PV-rich distribution systems. Int J Electr Power Energy Syst 2020;120:105997. http://dx.doi.org/10.1016/j.ijepes.2020.105997.

[4] Fu A, Cvetković M, Palensky P. Distributed cooperation for voltage regulation in future distribution networks. IEEE Trans Smart Grid 2022;13(6):4483–93. http://dx.doi.org/10.1109/TSG.2022.3191389.

[5] Fusco G, Russo M. A decentralized approach for voltage control by multiple distributed energy resources. IEEE Trans Smart Grid 2021;12(4):3115–27.

[6] Khayat Y, Shafiee Q, Heydari R, Naderi M, Dragičević T, Simpson-Porco JW, et al. On the secondary control architectures of AC microgrids: An overview. IEEE Trans Power Electron 2019;35(6):6482–500.

[7] Antoniadu-Plytaria K, Kouveliotis-Lysikatos I, Georgilakis P, Hatziargyriou N. Distributed and decentralized voltage control of smart distribution networks: Models, methods, and future research. IEEE Trans Smart Grid 2017;8(6):2999–3008.

[8] Mahmud N, Zahedi A. Review of control strategies for voltage regulation of the smart distribution network with high penetration of renewable distributed generation. Renew Sustain Energy Rev 2016;64:582–95.

[9] Fusco G, Russo M, De Santis M. Decentralized voltage control in active distribution systems: Features and open issues. Energies 2021;14(9):2563. http://dx.doi.org/10.3390/en14092563, URL: https://www.mdpi.com/1996-1073/14/9/2563.

[10] Lundberg M, Samuelsson O, Hillberg E. Local voltage control in distribution networks using PI control of active and reactive power. Electr Power Syst Res 2022;212:108475. http://dx.doi.org/10.1016/j.epsr.2022.108475.

[11] Nowak S, Wang L, Metcalfe MS. Two-level centralized and local voltage control in distribution systems mitigating effects of highly intermittent renewable generation. Int J Electr Power Energy Syst 2020;119:105858. http://dx.doi.org/10.1016/j.ijepes.2020.105858.

[12] Zhu J, Yuan Y, Wang W. Multi-stage active management of renewable-rich power distribution network to promote the renewable energy consumption and mitigate the system uncertainty. Int J Electr Power Energy Syst 2019;111:436–46. http://dx.doi.org/10.1016/j.ijepes.2019.04.028.

[13] Kontis EO, Kryonidis GC, Nousdilis AI, Malamaki K-ND, Papagiannis GK. A two-layer control strategy for voltage regulation of active unbalanced LV distribution networks. Int J Electr Power Energy Syst 2019;111:216–30. http://dx.doi.org/10.1016/j.ijepes.2019.04.020.

[14] Li P, Wei M, Ji H, Xi W, Yu H, Wu J, et al. Deep reinforcement learning-based adaptive voltage control of active distribution networks with multi-terminal soft open point. Int J Electr Power Energy Syst 2022;141:108138. http://dx.doi.org/10.1016/j.ijepes.2022.108138.

[15] Mahdi Noori R.A. S, Scott P, Mahmoodi M, Attarha A. Data-driven adjustable robust solution to voltage-regulation problem in PV-rich distribution systems. Int J Electr Power Energy Syst 2022;141:108118. http://dx.doi.org/10.1016/j.ijepes.2022.108118.

[16] Bolognani S, Carli R, Cavraro G, Zampieri S. On the need for communication for voltage regulation of power distribution grids. IEEE Trans Control Netw Syst 2019;6(3):1111–23. http://dx.doi.org/10.1109/TCNS.2019.2921268.

[17] Jahangiri P, Aliprantis D. Distributed Volt/Var control by PV inverters. IEEE Trans Power Syst 2013;28(3):3429–39.

[18] Farivar M, Chen L, Low S. Equilibrium and dynamics of local voltage control in distribution systems. In: 52nd IEEE conference on decision and control. 2013, p. 4329–34. http://dx.doi.org/10.1109/CDC.2013.6760555.

[19] Andrén F, Bletterie B, Kadam S, Kotsampopoulos P, Bucher C. On the stability of local voltage control in distribution networks with a high penetration of inverter-based generation. IEEE Trans Ind Electron 2015;62(4):2519–29.

[20] Zhu H, Liu HJ. Fast local voltage control under limited reactive power: Optimality and stability analysis. IEEE Trans Power Syst 2016;31(5):3794–803. http://dx.doi.org/10.1109/TPWRS.2015.2504419.

[21] Fusco G, Russo M. A procedure to determine the droop constants of voltage controllers coping with multiple DG interactions in active distribution systems. Energies 2020;13(8):1935. http://dx.doi.org/10.3390/en13081935, URL: https://www.mdpi.com/1996-1073/13/8/1935.

[22] Singhal A, Ajjarapu V, Fuller J, Hansen J. Real-time local Volt/Var control under external disturbances with high PV penetration. IEEE Trans Smart Grid 2019;10(4):3849–59. http://dx.doi.org/10.1109/TSG.2018.2840965.

[23] Bedawy A, Yorino N, Mahmoud K, Lehtonen M. An effective coordination strategy for voltage regulation in distribution system containing high intermittent photovoltaic penetrations. IEEE Access 2021;9:117404–14. http://dx.doi.org/10.1109/ACCESS.2021.3106838.

[24] Khorramabadi S, Bakhshai A. Critic-based self-tuning PI structure for active and reactive power control of VSCs in microgrid systems. IEEE Trans Smart Grid 2015;6(1):92–103.

[25] Mahmud N, Zahedi H, Mahmud A. ANFISPID-based voltage regulation strategy for grid-tied renewable DG system with ESS. In: 2016 IEEE innovative smart grid technologies - Asia. 2016, p. 81–6.

[26] Vu T, Lee M. Independent design of multi-loop PI/PID controllers for interacting multivariable processes. J Process Control 2010;20:922–33.

[27] Xiong Q, Cai W. Effective transfer function method for decentralized control system design of multi-input multi-output processes. J Process Control 2006;16:773–84.

[28] Yazdani A, Di Fazio AR, Ghoddami H, Russo M, Kazerani M, Jatskevich J, et al. Modeling guidelines and a benchmark for power system simulation studies of three-phase single-stage PhotoVoltaic systems. IEEE Trans Power Deliv 2011;26(2):1247–64.

[29] Ranamuka D, Agalgaonkar AP, Muttaqi KM. Examining the interactions between DG units and voltage regulating devices for effective voltage control in distribution systems. IEEE Trans Ind Appl 2017;53(2):1485–96. http://dx.doi.org/10.1109/TIA.2016.2619664.

[30] Ashabani M, Yasser A-RM, Mirsalim M, Aghashabani M. Multivariable droop control of synchronous current converters in weak grids/microgrids with decoupled dq-axes currents. IEEE Trans Smart Grid 2015;6(4):1610–20.

[31] Kammer C, Karimi A. Decentralized and distributed transient control for microgrids. IEEE Trans Control Syst Technol 2019;27(1):311–22.

[32] Ashabani M, Mohamed YA-RI, Mirsalim M, Aghashabani M. Multivariable droop control of synchronous current converters in weak grids/microgrids with decoupled dq-axes currents. IEEE Trans Smart Grid 2015;6(4):1610–20. http://dx.doi.org/10.1109/TSG.2015.2392373.

[33] Zhang Z, Ochoa L, Valverde G. A novel voltage sensitivity approach for the decentralized control of DG plants. IEEE Trans Power Syst 2018;3(2):1566–76.

[34] Casolino GM, Losi A. Load Area application to radial distribution systems. In: 2015 IEEE 1st international forum on research and technologies for society and industry, RTSI 2015 - Proceedings. 2015, p. 269–73. http://dx.doi.org/10.1109/RTSI.2015.7325109.

[35] Fusco G, Russo M. Robust MIMO design of decentralized voltage controllers of PV systems in distribution networks. IEEE Trans Ind Electron 2017;64(6):4610–20.

[36] Di Fazio AR, Russo M, Valeri S, De Santis M. Linear method for steady-state analysis of radial distribution systems. Int J Electr Power Energy Syst 2018;99:744–55.

[37] Bristol E. On a new measure of interaction for multi-variable process control. IEEE Trans Automat Control 1966;AC-11(1):133–4.

[38] Garcia-Sanz M. Robust control engineering: Practical QFT solutions. CRC Press; 2017.

[39] Chen P, Liu Y, Zhang W, Bao J. Analytical design and tuning method of multivariable controller for multi-input-multi-output (MIMO) processes. In: 2007 American control conference. IEEE; 2007, p. 651–6.

[40] Centre MHR. PSCAD user's guide. Manitoba Hydro International Ltd. 2018, URL: https://www.pscad.com.

[41] Yazdani A, Di Fazio AR, Ghoddami H, Russo M, Kazerani M, Jatskevich J, et al. Modeling guidelines and a benchmark for power system simulation studies of three-phase single-stage photovoltaic systems. IEEE Trans Power Deliv 2010;26(2):1247–64.